Quaternary Science Reviews 369 (2025) 109605

Contents lists available at ScienceDirect

Quaternary Science Reviews

journal homepage: www.elsevier.com/locate/quascirev

Past fire severity and intensity identified in SE Australian sediments using boron isotopes and FTIR spectroscopy

Rebecca Ryan [a,*], Shawn Lu [a], Damien Lemarchand [b], Zoë Thomas [c,d], Ivan Simkovic [e], Pavel Dlapa [e], Martin Worthy [f], Robert Wasson [f,g], Ross Bradstock [h], Katharine Haynes [h], Anthony Dosseto [a,h]

[a] Wollongong Isotope Geochronology Laboratory, School of Science, University of Wollongong, NSW, 2522, Australia
[b] Institut Terre et Environnement de Strasbourg, Université de Strasbourg-EOST, CNRS, ENGEES, 5 Rue René Descartes, 67084, Strasbourg Cedex, France
[c] Chronos 14Carbon-Cycle Facility, Mark Wainwright Analytical Centre, University of New South Wales, NSW, 2052, Australia
[d] School of Geography and Environmental Science, University of Southampton, Southampton, SO17 1BJ, United Kingdom
[e] Department of Soil Science, Faculty of Natural Sciences, Comenius University, Mlynská Dolina B-2, 842 15, Bratislava, Slovak Republic
[f] Fenner School of Environment and Society, Australian National University, Canberra, Australia
[g] College of Science and Engineering, James Cook University, Cairns, Queensland, Australia
[h] Centre for Environmental Risk Management of Bushfires, University of Wollongong, Wollongong, NSW, 2522, Australia

ARTICLE INFO

Handling Editor: Dr Yan Zhao

Keywords:
FTIR spectroscopy
Isotopes
Fire
Southeastern Australia
Fire intensity

ABSTRACT

Landscape-scale bushfires threaten lives, property, and biodiversity. Understanding how their characteristics have changed over time proves vital in improving management strategies and understanding future ecosystem responses. Therefore, there is an urgent need to develop novel proxies to extend our existing record of past fire characteristics, such as severity and intensity. Here, we use carbon and nitrogen contents, Fourier Transform Infrared (FTIR) spectroscopy, and boron isotopes in a sedimentary archive to investigate past fire events in Namadgi National Park (southeastern Australia) and estimate their characteristics such as fire intensity and severity. Strontium and neodymium isotopes were used to assess the possible catchment-scale erosion events following fire. The aromatic/aliphatic ratio of sediments showed that fire frequency and intensity have increased in the last 200 years compared to the previous 3000. Boron isotopes were influenced by both lithology and fire severity, where negative excursions may result from higher contributions of bark to mineral ash, whilst positive excursions in the isotope ratio result from higher contributions of leaves. Negative excursions in the B isotope ratio, coinciding with positive excursions in the aromatic/aliphatic ratio, were hypothesised to record low-severity fires that experienced longer residence times. This multi-proxy approach provides valuable insights into past fire characteristics. By improving our understanding of how fire characteristics have changed in the past, the results can inform mechanistic models to improve predictions of fire severity and intensity changes in the future.

1. Introduction

As climate change continues to result in the increased frequency and duration of extreme fire weather conditions, the threat of more high-severity and intensity fire events has become an increasing concern (Collins et al., 2021; Nolan et al., 2021a). This has implications for ecosystem response, fire management and water quality (Driscoll et al., 2024; Nolan et al., 2021b; White et al., 2006). Fire severity is defined as the degree of canopy consumption, ranging from low, where the flames are confined to the understorey, to extreme, where the canopy is completely consumed (Hammill and Bradstock, 2006; Keeley, 2009; McLauchlan et al., 2020). Intensity describes the energy output or the heat transfer of the fire (Keeley, 2009; McLauchlan et al., 2020). Plants are not adapted to fire as such, rather, they are adapted to the fire regime, which incorporates frequency, intensity, type, and seasonality (Bowman et al., 2014). The dominant vegetation species of the catchment will determine the ability of the ecosystem to regenerate following fire events. For example, in rainforest environments, high-severity fire

* Corresponding author. Wollongong Isotope Geochronology Laboratory, School of Science, University of Wollongong, NSW, 2522, Australia.
E-mail address: rjryan@caltech.edu (R. Ryan).

https://doi.org/10.1016/j.quascirev.2025.109605
Received 16 April 2025; Received in revised form 8 July 2025; Accepted 28 August 2025
Available online 1 September 2025

events can cause significant tree mortality, however, eucalypt forests regenerate quickly even after extreme fire conditions (Clarke et al., 2014). Fire events of different severities and intensities can also increase the hydrophobicity of the soil, increasing the potential for surface runoff and in-washing of fine sediments and nutrients to waterways (Leigh et al., 2015; White et al., 2006). This can have significant impacts on water quality. Therefore, understanding how fire severity and intensity have changed over time is important for predicting how the catchment may respond to future fire events.

Current records of past fire events employ techniques such as palynology, charcoal analysis and cambial scars in dendrochronological reconstructions (e.g. Hennebelle et al., 2020; Mooney and Tinner, 2011; Rowe et al., 2019; Zylstra, 2006). More recently, remote sensing data has allowed for high-resolution reconstructions of past fire characteristics (e.g. Chafer, 2008; Gibson et al., 2020; Malone et al., 2011). However, these images are restricted to the last 30–50 years within the satellite era (Chuvieco and Congalton, 1989). In order to more accurately predict the characteristics of future fire events, there is a need to extend our existing fire record.

Fourier Transform Infrared (FTIR) spectroscopy is a semi-quantitative technique that uses infrared light to determine the amount of incident light absorbed at specific wavenumbers (Beasley et al., 2014; Griffiths, 1990). Increased temperature and changes in oxygen availability, such as during pyrolysis, result in the transformation, destruction, and creation of bonds (Dlapa et al., 2013). By analysing the changes in chemical composition using FTIR spectroscopy, it is possible to understand the characteristics of the fire. FTIR has been successfully applied to charcoal samples (Gosling et al., 2019; Constantine IV et al., 2021; Maezumi et al., 2021; Constantine IV, Williams et al., 2023; Constantine IV, Zhu et al., 2023), soils (Lu et al., 2022; Simkovic et al., 2008; Šimkovic et al., 2023) and sediments (Ryan et al., 2023, 2024, 2025). Aliphatic bonds typically undergo thermal decomposition during a fire event due to exposure to high temperatures and/or prolonged heating durations (Abakumov et al., 2018). This results in a relative increase in aromatic bonds through Diels-Alder-type reactions (Araya et al., 2017; Guo and Bustin, 1998; Rausa et al., 1999). A ratio of aromatic/aliphatic bonds has been shown to be a promising indicator of high-intensity fire events in sediment deposits (Ryan et al., 2023, 2024, 2025). Mineral bonds typically require higher temperatures for transformation than organic components (Araya et al., 2017; de Santana et al., 2006). This also imparts changes in the FTIR spectra, which can provide estimates of the approximate temperatures reached during the fire. Therefore, the aromatic/aliphatic ratio of sediments can be used to assess the intensity of past fire events.

Boron is an essential micronutrient for plants, performing a key role in cell wall formation, sugar transport, and nitrogen assimilation (Blevins and Lukaszewski, 1998; Mateo et al., 1986; Ruiz et al., 1998) and varies over a narrow range between toxicity and deficiency (Goldberg et al., 2005). Boron has two stable isotopes, ^{10}B and ^{11}B, and their ratio is expressed as the $\delta^{11}B$ value. It undergoes significant isotope fractionation in vegetation. Soil solution is uptaken by plant roots via passive diffusion with minimal fractionation (Chetelat et al., 2021; Cividini et al., 2010; Roux et al., 2022). However, as the soil solution is transported via the xylem to the leaves, it becomes progressively enriched in ^{11}B as ^{10}B becomes structurally bound (Park and Schlesinger, 2002; Roux et al., 2022). Ash from combusted leaves has shown greater enrichment in the heavier isotope, resulting in higher $\delta^{11}B$ values for the clay-sized fraction of soils burnt in at least one high-severity fire (Lu et al., 2022, 2024). Sediments recording a known high-severity fire event have shown a higher $\delta^{11}B$ value, suggesting leaching of the ash and transportation to sediment reservoirs (Ryan et al., 2023). Conversely, when ash from combusted bark reacts with rainwater, simulating a low-severity fire, it results in a reduced $\delta^{11}B$ value of the leaching solution and, subsequently, the clay fraction of soils that have been in contact with the solution (Lu et al., 2022). It is, therefore, hypothesised that B isotopes can be used in sediment deposits to assess past fire severity.

This study applies a multi-proxy approach of B isotopes and FTIR spectroscopy to evaluate the severity and intensity of past fire events in Namadgi National Park, a known fire-prone landscape in southeastern Australia and assess changes in these characteristics over time. It is expected that sediments recording fires that burnt at high severity and intensity will show increases in the $\delta^{11}B$ value and the aromatic/aliphatic ratio, respectively, compared to sediments that do not record fire events. Carbon and nitrogen contents were paired with the two proxies (B isotopes and FTIR) to gain an understanding of changes to organic matter quality over time and with exposure to fire, and strontium and neodymium isotopes were used to assess sediment transport from different parent materials to infer changes to catchment-scale erosion events as a result of the fire events recorded.

2. Methods

2.1. Study area

Namadgi National Park is located approximately 50 km west of Canberra, covering just over 1000 km^2 (Salmona et al., 2018). The Cotter Catchment within Namadgi National Park is one of two principal water supplies for Canberra, and the Cotter River is regulated by 3 dams: Bendora, Corin and Cotter (Nichols et al., 2006; Worthy, 2005). Rainfall in the catchment averages 900–1000 mm/year (Nichols et al., 2006; Worthy, 2005). This can be significantly reduced in extreme drought years, resulting in increased available fuel loads and altered bushfire dynamics (Worboys, 2003). The catchment is characterised by dry sclerophyll forests dominated by eucalypt species, and subalpine woodland (Dixon et al., 2018; Pryor, 1939). The soils developed from acidic, volcanic rocks, which are typically shallow and highly erodible once disturbed (Carey et al., 2003; Granged et al., 2011). Granites are dominant along the ridgelines, whilst Ordovician shales, sandstones and clays are present on the slopes (Nichols et al., 2006). The soils developed on these rocks are commonly lithosols with minimal profile development.

Prior to the 2003 and 2019–20 bushfires, the Cotter Catchment experienced major fire events in 1920, 1926 and 1939 (Daniell and White, 2005). The 1939 fire was reported to be particularly severe due to strong winds, which resulted in spot fires up to 24 km ahead of the firefront (Carey et al., 2003; Daniell and White, 2005). The 2003 bushfire was first ignited by electrical storms on the January 8, 2003; however, on the January 17, 2003, extreme fire weather characterised by high temperatures, very low relative humidity, and strong wind gusts significantly increased the fire intensity (Carey et al., 2003). Over 1000 km^2 was burnt in the proceeding 36 h, much of which was national park, and burnt through threatened Alpine Ash (*Eucalyptus delegatensis*) communities (Carey et al., 2003). In addition, four lives were lost and over 500 houses were destroyed during the extreme fire weather conditions of the 2003 bushfires (Worboys, 2003).

Here, we analysed samples from the floodplain of the Cotter River (CR-01), where it is joined by De Salis Creek (Fig. 1), to determine how the sediment chemistry has changed through time in response to fire events. Remote sensing data suggests that this site was only burnt during the 2003 and 2019–20 fires in the period from 1950 to present. Soil samples were also collected less than one year following the 2019–20 bushfires and represent a range of fire severities experienced during this event. The soil samples are further divided by lithology and are derived from the two predominant bedrock types in the catchment: metasedimentary and granodiorite (Fig. 1).

2.2. Sample collection

A 75 mm diameter sediment core was collected from the riverbank marking the start of the floodplain at the CR-01 site (35.610396°S, 148.822151°E, WGS84; Fig. 1), to a depth of 77.5 cm. The vegetation

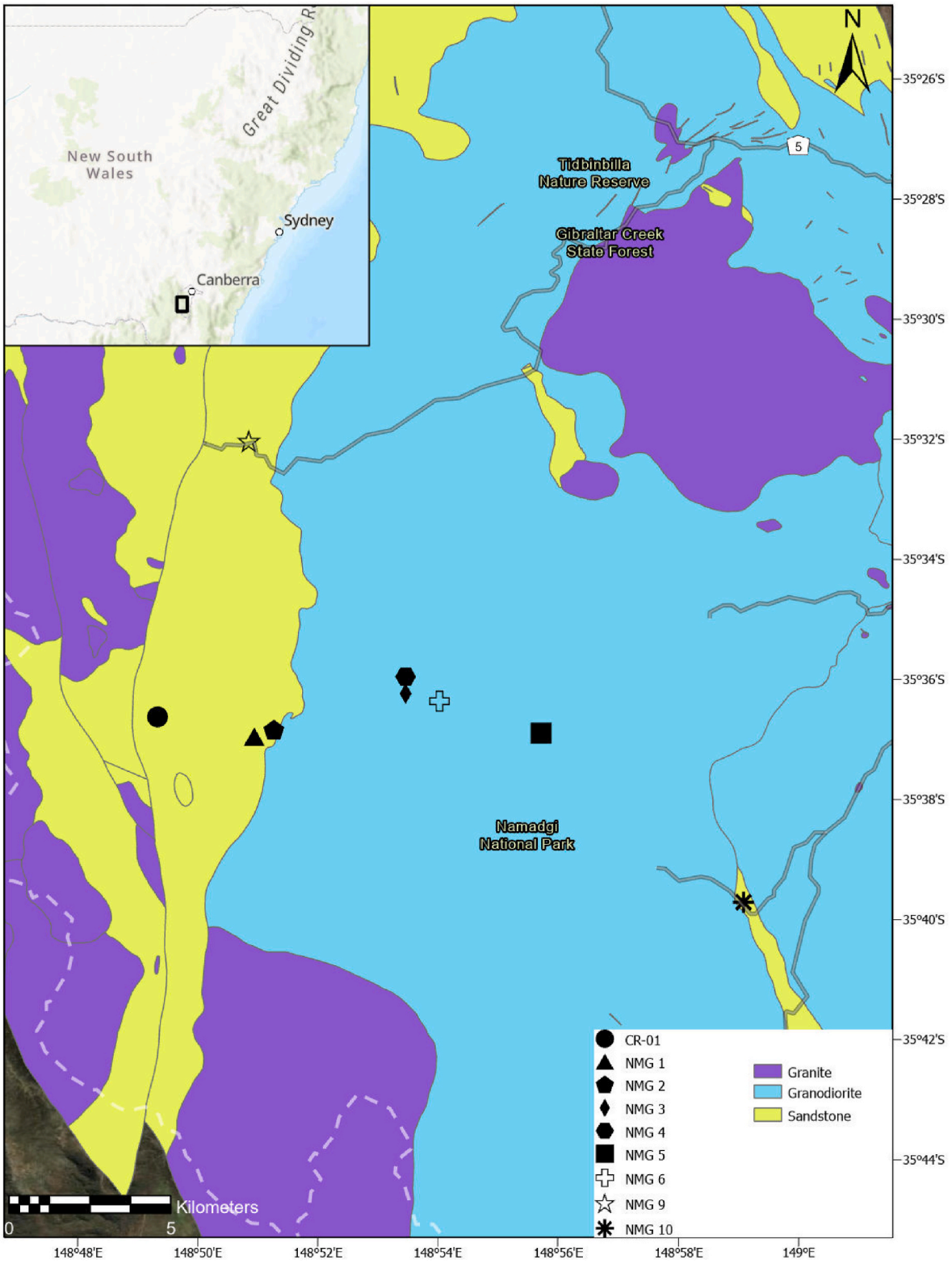

Fig. 1. A simplified geological map of Namadgi National Park in southeastern Australia, highlighting the location of the Cotter River Core (CR-01, circle) and the soil samples derived from different bedrock types (NMG1-6 and NMG 9–10). NMG codes with an open symbol denote soil samples, and a closed symbol represents soil and bedrock samples. Geological data adapted from Department of Regional New South Wales' NSW Seamless Geology' dataset, 2022. Satellite Image: Esri, Maxar, GeoEye, Earthstar Geographics, CNES/Airbus DS, USDA, USGS, AeroGRID, IGN and the GIS User Community Esri, HERE, Garmin, © OpenStreetMap contributors and the GIS User Community. Inset: Esri, HERE, Garmin, Intermap, increment P Corp., GEBCO, USGS, FAO, NPS, NRCAN, GeoBase, IGN, Kadaster NL, Ordnance Survey, Esri Japan, METI, Esri China (Hong Kong), (c) OpenStreetMap contributors, and the GIS User Community.

immediately to the west of the site was characterised by dry sclerophyll forest. The river is situated approximately 5 m to the east of the coring site. Half of the core was subsampled at a resolution of 1 cm for analysis. Eleven soil samples were also collected from local topographic highs across the Cotter River Catchment and analysed for B isotopes. A subset of six of the soil samples were also analysed for Sr and Nd isotopes. The samples were collected from soils developed on both metasedimentary and granodiorite parent material and in areas that experienced low, high and extreme fire severity during the 2019–2020 fires. Granodiorite and metasedimentary bedrock samples were collected from rock outcrops adjacent to soil sampling sites NMG 6 and NMG 9, respectively and ground to a fine powder for Sr and Nd isotope analysis.

2.3. Age-depth model determination

Four charcoal sub-samples from the CR-01 core were handpicked for radiocarbon dating. Dating was performed by Accelerated Mass Spectrometry (AMS) at the Chronos ^{14}Carbon-Cycle Facility, UNSW. Samples were pre-treated using an acid-base-acid pre-treatment in 1M HCl and 0.2M NaOH at 80 °C for 20 min before graphitisation following Turney et al. (2021). Twenty-five optically stimulated luminescence (OSL) dates had previously been determined by Worthy (2013). For the OSL analysis, quartz grains between 180 and 212 μm were isolated and acid-washed with HCl and HF. Where necessary, heavy minerals were removed using sodium polytungstate. Samples were then leached with HF combined with a small volume of HCl to avoid calcium fluoride formation. Samples were analysed using a Risø TL-DA-15 Min-iSys II at the Australian National University. Single-grain measurements were made using the 532 nm laser, and all signals were detected using an EMI 9235QA PMT filter. The beta dose rate for each subsample was calculated using ICP-MS measurement of U, Th and K content, and the gamma dose rate used was simply twice the measured 2π geometry measurement at the surface of each subsample. The subsample depth was used to calculate the cosmic dose rate contribution using the formulae of Prescott and Hutton (1994). The equivalent dose (assuming equilibrium in the isotopes of U, Th and K) was calculated with the Analyst software (version 3.24), and the minimum age model ages were used in conjunction with the radiocarbon dates for the age-depth model.

The radiocarbon and OSL ages were input into Oxcal 4.4, a Bayesian model employing Markov Chain Monte Carlo simulations (Bronk Ramsey, 2009). The 'P_sequence deposition model' was used with the charcoal outlier model applied to the charcoal samples (Bronk Ramsey, 2009). The OSL dates were converted to the appropriate format for incorporation into the age-depth model. The year of sampling at 0 cm was input into the model as an upper constraint. The 'SHCal 20′ and 'Bomb 21 SH12′ calibration curves were used to generate a cal BP age-depth model (Hogg et al., 2020; Hua et al., 2021).

2.4. Carbon and nitrogen

Carbon (C) and nitrogen (N) contents in the core sediments were measured using an Elementar Vario Macro Cube Element Analyser at the Wollongong Isotope Geochronology Laboratory (WIGL). Approximately 100 mg of the bulk sub-samples were ground to a fine consistency, and ~50 mg was used for analysis. Three phenylalanine standards of different masses were analysed to create a calibration curve at the start of the sequence. Two blanks were analysed before, and one after the phenylalanine standards were analysed, and had C and N area values of <300. A repeat was analysed every 8 samples (n = 9) to assess precision, giving 2 standard error (SE) values of ±0.09, ±0.01 and ± 0.53 for C, N and C/N ratio, respectively. A phenylalanine standard was analysed every 10 to 15 samples to account for drift. Carbon and N concentrations are reported as weight percent (wt %), and the C/N ratio is unitless.

2.5. FTIR spectroscopy

All sediment samples (n = 77) and replicates (n = 4) from the CR-01 core were analysed for FTIR spectroscopy by KBr pressed discs at Comenius University, Slovakia, using a Nicolet 6700 FTIR spectrometer and OMNIC 8 software (Thermo Fisher Scientific). Approximately 1 g of the bulk sediment of each sample was ground to a fine, homogenous powder using a zirconium oxide mill and then dried at 60 °C for 24 h. 2 mg of each sample was combined with 200 mg of KBr and pressed into a pellet. Measurements were conducted in transmission mode across the 4000–400 cm^{-1} range. One hundred and twenty-eight scans were averaged for each sample at a resolution of 2 $cm^{-1,}$ and the results were reported in absorbance values. The averaged spectra were baseline corrected in Python 3.8 using the 'arPLS' method (Baek et al., 2015) in the 'RamPy' package (Le Losq, 2018). The baseline-corrected spectra were analysed for changes in peak height and peak area ratios, determined by taking the area under the curve for the bands of interest, including the aromatic (1750–1500 cm^{-1}), aliphatic (3000–2800 cm^{-1}) and inorganic (750–600 cm^{-1}) bands. Due to the long duration of the record, a change point analysis was performed using the "ggchangepoint" package in RStudio (Killick and Eckley, 2014) to identify key periods of significant change in the aromatic/aliphatic ratio. Significant increases in the aromatic/aliphatic peak area ratio were identified at >2 standard deviations (SD) from the mean. Changes in the aromatic/inorganic ratio were used to determine layers of higher organic matter contributions.

2.6. Boron isotopes

The clay-sized fraction of sediments from the CR-01 core, as well as of 11 soil samples were prepared and analysed for B isotopes at WIGL. Approximately 50 mg of each sub-sample was combined with potassium carbonate in a 1:5 flux for alkali fusion at 950 °C. The resulting solid was dissolved in HCl and 18.2 M-Ω water by sonication, and the supernatant was isolated by centrifugation for chromatography. A two-step ion chromatography method was employed to isolate B for isotopic analysis (Lemarchand et al., 2012). First, 5 mL of solution was loaded onto a column containing 1.5 mL of BIORAD AG50W-X8 resin for cation exchange chromatography. Boron is not retained on the resin and was collected during sample loading. The pore solution was flushed with 2 mL of 0.01 M HCl. The resulting solution was then pH-adjusted to 8–10 using 0.5 M NaOH that was previously purified using a column loaded with Amberlite IRA 743 resin. Each sample was then loaded onto a column containing 0.5 mL of Amberlite IRA 743 resin. The matrix was eluted in water. Sodium chloride was then loaded to replace anions with chlorine, and an additional matrix elution with water removed sodium. Boron was then eluted in 0.5 M HCl.

Boron isotopes were measured by multi-collector inductively coupled plasma mass spectrometry (MC-ICP-MS) with a ThermoFisher Neptune Plus™ at WIGL. The sample introduction system consisted of a standard sample and H skimmer cone, a PFA nebuliser with a flow rate of approximately 100 μL min^{-1} and a Scott Cyclonic Spray Chamber. ^{10}B and ^{11}B were collected in Faraday cups coupled with a 10^{11}-Ω resistor. Tuning was performed to gain a sensitivity of 0.5 V of ^{11}B per 50 ppb of B in the primary standard, NIST SRM 951a. Measurements were performed in low-resolution mode. Standard-sample-standard bracketing was used to correct for mass bias. ERM AE120 was analysed as a secondary standard at the beginning and end of each analysis sequence. The total procedure blank was 8.1 ± 1.1 ng B (2SE; n = 9). The mean measured δ^{11}B values for ERM AE120 was −20.44 ± 0.12 ‰ (2SE; n = 17), which is within error of the expected value (−20.2 ± 0.6 ‰; Vogl and Rosner, 2012). Mean measured δ^{11}B values for USGS W2-a reference material was 11.44 ± 0.41 ‰ (2SE; n = 8) which is within error of the recommended value (12.2 ± 0.4 ‰; Gangjian et al., 2013). Precision was assessed by analysing replicate sediment (n = 3) and soil (n = 4) samples, giving a 2SE of ±0.3 ‰ and ±0.5 ‰, respectively.

2.7. Strontium and neodymium isotopes

Strontium and Nd isotopes were analysed on two bedrock samples (metasedimentary and granodiorite) as well as six soil samples, three developed over each bedrock type, and 16 core sediment samples, representing a range of B isotope ratios and depths. Approximately 30 mg of each sample and USGS BCR-2 reference material were dissolved in HF and HNO_3, followed by aqua regia and H_2O_2. The samples were redissolved in 2M HNO_3 prior to ion exchange chromatography. Chromatography was performed using a prepFAST-MC™ (Elemental Scientific) following Retzmann et al. (2017). Samples were loaded in 1 mL of 2M HNO_3. Strontium was eluted in 4 mL of 0.2 M HNO_3. Due to poor Nd recovery, samples were eluted in 1.7 M HCl, instead of the usual 2 M HCl typically used in Retzmann et al. (2017).

Strontium and Nd isotopes were measured by MC-ICP-MS at WIGL using a ThermoFisher Neptune Plus™ at WIGL. The sample introduction system consisted of a jet sample and H skimmer cone (Nd isotopes) or jet sample and x skimmer (Sr isotopes) cones, a PFA nebuliser with a flow rate of approximately 100 μL min^{-1}, and a Scott Cyclonic Spray Chamber. Tuning was performed to gain a sensitivity of 1.4 V of ^{142}Nd per 200 ppb of Nd in the primary standard, JNDi-1 and 6 V of ^{88}Sr per 50 ppb of Sr in NIST SRM 987. Measurements of both elements were performed in low-resolution mode. Instrument mass bias was internally corrected using $^{88}Sr/^{86}Sr$ and $^{146}Nd/^{144}Nd$, respectively. Isobaric interferences between $^{87}Sr^{+}$ and $^{87}Rb^{+}$ were internally corrected by monitoring $^{83}Kr/^{84}Sr$, $^{83}Kr/^{86}Sr$ and $^{85}Rb/^{87}Sr$. Isobaric interferences between $^{144}Nd^{+}$ and $^{144}Sm^{+}$ were internally corrected by monitoring $^{147}Sm/^{144}Nd$, $^{147}Sm/^{148}Nd$, $^{147}Sm/^{150}Nd$ and $^{140}Ce/^{142}Nd$. The total procedure blank was 168 ng of Nd and 40 pg of Sr. Measured values for BCR-2 were 0.512463 ± 0.000008 and 0.70458 ± 0.000002 for $^{143}Nd/^{144}Nd$ and $^{87}Sr/^{86}Sr$, respectively, which are both lower than reported values in Jweda et al. (2016) ($^{143}Nd/^{144}Nd$: 0.512637 ± 0.000013, $^{87}Sr/^{86}Sr$: 0.705000 ± 0.000011). Reduced accuracy may be due to the age of the resin; however, since we are assessing general trends with increasing depth, lower accuracy does not affect the overall trend detected. Precision was assessed by analysing a replicate sample (n = 1) with 2SE values of ±0.000020 and ± 0.0053 for $^{143}Nd/^{144}Nd$ and $^{87}Sr/^{86}Sr$, respectively. Lower precision on the Sr isotope ratio may be due to higher sample heterogeneity. The $^{143}Nd/^{144}Nd$ are reported as both raw ratios and in εNd notation using the modern chondritic composition (CHUR) value of 0.512638 (Jacobsen and Wasserburg, 1980).

3. Results

3.1. Age-depth model

Three radiocarbon ages and 25 OSL dates were used to determine the age-depth model for the CR-01 site (Supplementary Table 1 and Fig. 2). One of the radiocarbon ages was identified as an outlier based on the posterior value from the outlier model and was not incorporated into the final age-depth model. The profile covers the last ~3000 years, with the sedimentation rate decreasing with increasing depth ranging from 0.02 cm/yr at the base of the core to 0.129 cm/yr at the surface (Supplementary Fig. 1B). Age uncertainties are small for most of the core (<200 years); however, uncertainties increase for ages older than ~2000 years (Supplementary Fig. 1A).

3.2. Carbon and nitrogen

The carbon (C) content of CR-01 core sediments ranges from 0.1 wt% (0–1 cm) to 9.78 wt% (74–75 cm) and follows a general decreasing trend with increasing depth (Fig. 3 A). Increases in the C content are evident at 0–1 cm, 17–18 cm and 30–31 cm, corresponding to −62 (+6/–11) cal yr BP, 70 (+44/–38) cal yr BP and 622 (+106/–104) cal yr BP, respectively, in the model (Supplementary Fig. 2A).

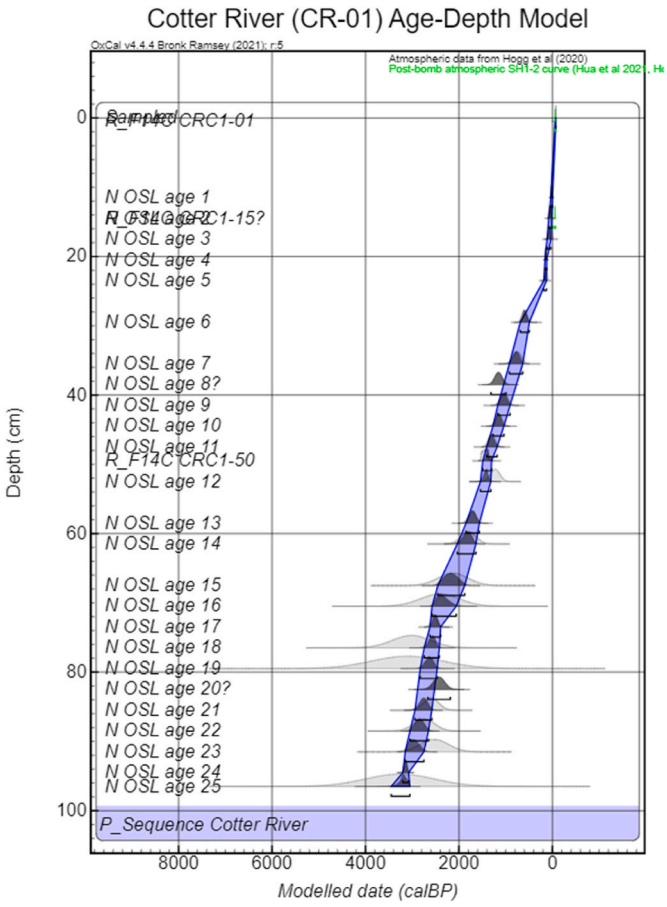

Fig. 2. Radiocarbon and OSL-based age-depth models from OxCal (Ramsey, 2006) for the Cotter River Core.

The nitrogen (N) content of CR-01 core sediments ranges from 0.02 wt% (38–39 cm) to 0.57 wt% (0–1 cm) and, like the C content, follows a general decreasing trend with increasing depth (Fig. 3B). Only two peaks are evident at 0–1 cm and 30–31 cm, corresponding to ages of −62 (+6/–11) cal yr BP and 622 (+106/–104) cal yr BP, respectively (Supplementary Fig. 2B).

The C/N ratio ranges from 1.15 (41–42 cm) to 35.17 (17–18 cm), with a general decreasing trend with increasing depth (Fig. 3C). Peaks are evident at 17–18 cm, 31–32 cm, 38–39 cm and 41–42 cm, corresponding to 70 (+44/–38) cal yr BP, 622 (+106/–104) cal yr BP, 909 ± 137 cal yr BP and 1042 (+127/–135) cal yr BP, respectively (Supplementary Fig. 2C).

3.3. FTIR spectroscopy

Aromatic to aliphatic ratios in the CR-01 sediments vary from 3.0 (17–18 cm) to 14.3 (14–15 cm). Due to the length of the record, a changepoint analysis was used to identify periods of significant change. Three regions were identified, and ratio values were classified as fire-affected layers at values > 10.7 (0–25 cm), >10.0 (25–52 cm), and >8.4 (52–77 cm), equivalent to >2SD from the mean (Fig. 4A). Peaks in the top ~23 cm, corresponding to the last ~200 years in the age-depth model, show the highest peak area ratio values, and the number of years between each of these peaks is shorter compared to the remainder of the core. The aromatic/inorganic ratio is consistent and low, with values ranging from 0.12 (63–64 cm) to 1.9 (0–1 cm).

Over the spectra, peak absorbance is highest in bands typically ascribed to mineral bonds (Supplementary Fig. 3). This is particularly evident at 466 cm^{-1}, ascribed to Si–O–Si deformation (Madejová and

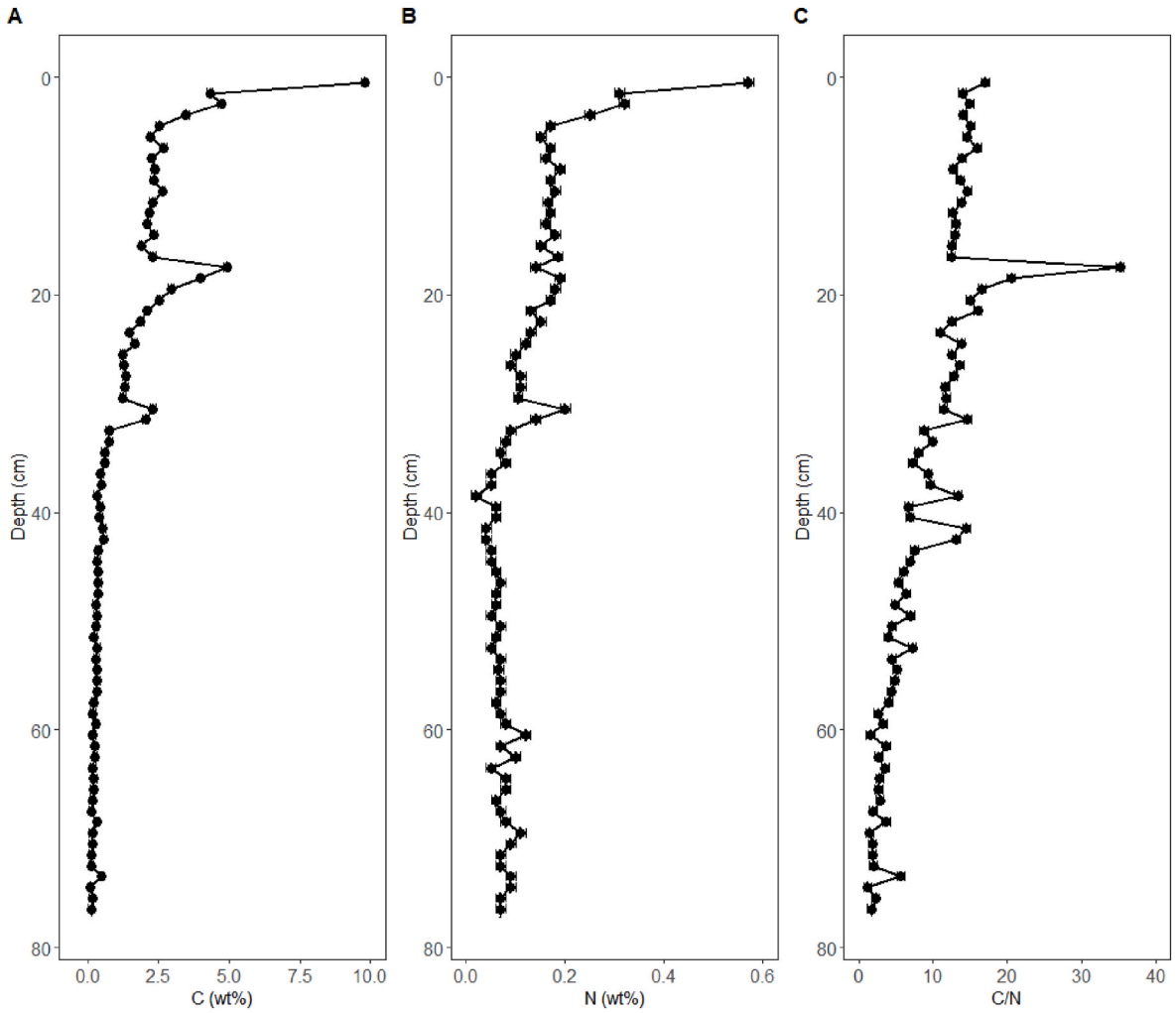

Fig. 3. A) C contents (in wt%), B) N contents (in wt%) and C) C/N ratio for CR-01 core sediments as a function of depth in the CR-01 core. Error bars are smaller than the symbol size.

Komadel, 2001), 536 cm^{-1}, associated with Fe–O bonds (Yusiharni and Gilkes, 2012) and the quartz doublet at 776 and 798 cm^{-1} (Madejová and Komadel, 2001). High peak absorbance is also evident in the peaks ascribed to the hydroxyl stretching vibrations of kaolinite, with peaks centred on 3620, 3650, and 3697 cm^{-1}, which results from proton bonding with Al^{3+} coordinated oxygen bonds in an octahedral site (Berna et al., 2007; Schroeder, 2002). The band at 1635 cm^{-1} is ascribed to C=O and asymmetric COO– vibrations of ketones, amides and carboxylic acids with aromatic C=C structures (Ellerbrock et al., 2005). Samples at 0–2 cm have the highest peak intensity in this band. Peak absorbance is low across all samples in the band at 2923 and 2852 cm^{-1}, ascribed to aliphatic C–H stretching of CH_3 or CH_2 groups (Dlapa et al., 2013; Hong et al., 2019). The highest peak intensities are found in the band at 1031–1008 cm^{-1}. This band is attributed to the aliphatic C–O and alcohol C–O stretching vibrations of cellulose (Guo and Bustin, 1998; Keiluweit et al., 2010), but can also be associated with asymmetric Si–O–Si stretching vibrations (Smidt et al., 2005). Given that bulk sediment samples were analysed, it is not possible to discount either possibility.

3.4. Boron isotopes

The $\delta^{11}B$ values vary from −10.68 ‰ (at a depth of 14–15 cm) to −0.80 ‰ (0–1 cm) in CR-01 sediments. There is a general decreasing trend with increasing depth over the top ~10 cm of the core (Fig. 4C, Supplementary Fig. 4B). Below 10 cm, values remain relatively constant except for positive and negative excursions. $\delta^{11}B$ excursions were identified as values that deviate by more than 2SD from the mean. Therefore, positive excursions were defined as values >–7.33 ‰ and negative excursions as values <–9.33 ‰. The largest positive excursions are observed at 0–4, 51–55, 74–75 and 76–77 cm depth (Fig. 4C). Additional positive excursions are also present at 22–23, 30–31, 64–65 and 70–71 cm depth. Negative excursions are evident at 14–15, 20–21, 26–27, 28–29, 33–34, 35–36, 44–45, 47–48 and 58–59 cm depth. There was no clear relationship between the $\delta^{11}B$ and B concentration (Supplementary Fig. 5).

The $\delta^{11}B$ value of soil samples ranges from −7.34 (metasedimentary, extreme severity) to 5.91 ‰ (granodiorite, high severity) (Fig. 5). In general, the $\delta^{11}B$ value is higher for samples developed on granodiorite bedrock compared to those on metasedimentary bedrock. Soils experiencing low and extreme severity fire show a similar trend across both bedrock types. However, high-severity events respond differently with bedrock type, showing a decreased $\delta^{11}B$ value for soils formed over metasedimentary bedrock and an increase for soils formed over granodiorite bedrock.

3.5. Strontium and neodymium isotopes

Bedrock samples yield $^{143}Nd/^{144}Nd$ ratios of 0.511870 ± 0.000020 (metasedimentary) and 0.512150 ± 0.000020 (granodiorite) (Table 1

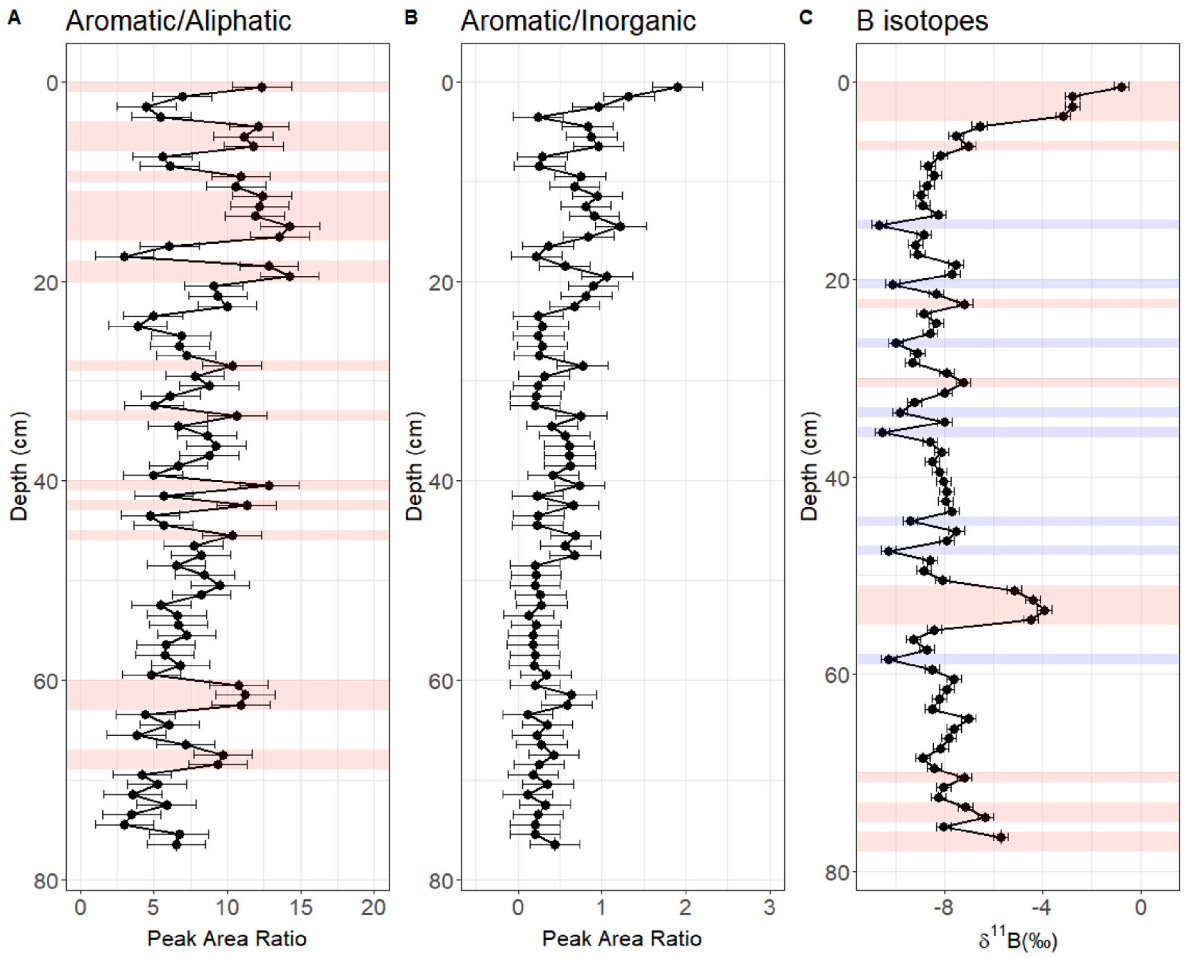

Fig. 4. A) Aromatic/aliphatic (A1750–1500 cm^{-1}/A3000–2800 cm^{-1}), B) aromatic/inorganic (A1750–1500 cm^{-1}/A750–600 cm^{-1}), and C) $\delta^{11}B$ value in per mill (‰) as a function of depth in cm in the Cotter River (CR-01) core. Red shading symbolises positive excursions whilst blue shading represents negative excursions. (For interpretation of the references to colour in this figure legend, the reader is referred to the Web version of this article.)

and Fig. 6A). The $^{143}Nd/^{144}Nd$ ratio of the soils developed over these two bedrock types ranges from 0.511956 to 0.512009 (εNd values of −13.31 to −12.28) in the metasedimentary-derived soils and 0.512069 to 0.512156 (εNd values of −11.11 to −9.41) for soils developed over granodiorite bedrock. Sediment samples from CR-01 display $^{143}Nd/^{144}Nd$ ratios intermediate to those in the two bedrock samples, ranging from 0.511984 (εNd: −12.75; 76–77.5 cm) to 0.512074 (εNd: −11.01; 30–31 cm). Sediments at the surface of the core display values similar to those observed in soils derived from granodiorite bedrock, whilst sediments at the bottom of the core show values closer to those observed in soils derived from metasedimentary bedrock. The $^{143}Nd/^{144}Nd$ ratios and $\delta^{11}B$ values seem to co-vary with depth (Fig. 6A–C).

The bedrock samples yield $^{87}Sr/^{86}Sr$ ratios of 0.925066 ± 0.000053 (metasedimentary) and 0.740255 ± 0.000053 (granodiorite) (Table 1 and Fig. 6B). Soil samples show ranges of 0.738097–0.779228 and 0.729900–0.763943 for soils derived from metasedimentary and granodiorite bedrocks, respectively. There is an overlap in the ranges for the Sr isotope values of soils developed over the two bedrock types. Sediments display $^{87}Sr/^{86}Sr$ ratios ranging from 0.750446 (76–77.5 cm) to 0.775228 (52–53 cm).

4. Discussion

In the soil clay samples, B isotope composition is predominantly controlled by the lithology. Soils developed on metasedimentary parent materials have $\delta^{11}B$ of ~ −9 to −4 ‰, while those developed on granodiorite parent materials have $\delta^{11}B$ ranging from ~ −4 to +6 ‰. Fire severity shows no systematic effect on the boron isotope compositions of soils developed on either lithology (Fig. 5). This contrasts with previous experiments showing that boron leached from combusted bark and leaves can impart boron isotopic signals in soil clay fractions that vary with fire severity (Lu et al., 2022, 2024). The lack of a relationship between boron isotope compositions in the soil and fire severity indicates that either no boron isotopic signal was imparted by varying fire severity at these sites or that any generated signal was subsequently removed or masked. This contradicts experimental observations, which have shown that ash from the combustion of tree leaves, which are isotopically heavier than lower plant compartments, such as trunk wood, bark and roots (Lu et al., 2024; Roux et al., 2022), is the key factor that may impart heavier boron isotope compositions to soils following higher-severity fires. However, it is possible that thermal updraft during wildfires could transport ash some distance away (Clark, 1988), thus preventing a boron isotope signal in the soil locally at our sites. In addition, our sites, which are located at the tops of hillslopes, could minimise the deposition of leaves and ash from trees in adjacent areas. In the absence of leaf ash, soils that experienced both low and high-severity fires could still incorporate B from charcoals, which are larger and less likely to be removed by thermal updraft. Bark charcoals tend to lower the $\delta^{11}B$ of soils (Lu et al., 2022, 2024), and the dynamic variation in the boron isotope composition of our soil samples could reflect the varying amount deposited and composition of ash and charcoal rather than fire severity (Fig. 5).

Erosion may also influence the retention of the B isotopic signature of

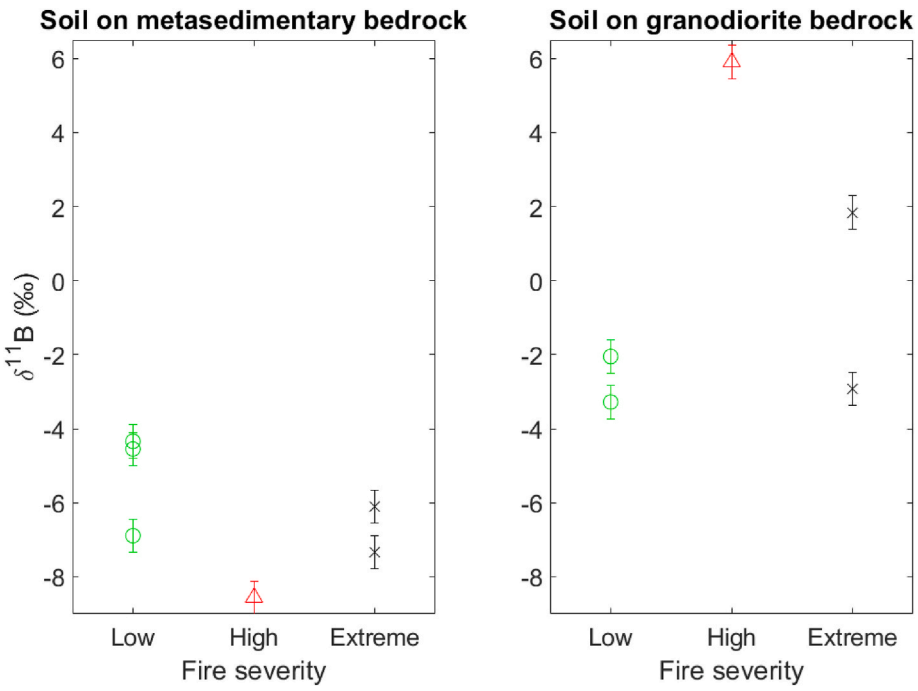

Fig. 5. $\delta^{11}B$ values of soils (top 10 cm) exposed to different fire severities during the 2019–20 bushfires, where the left panel shows data for soils developed on metasedimentary bedrock and the right panel shows data for soils developed on granodiorite bedrock.

Table 1
Nd and Sr isotope composition of soil, sediment and bedrock samples from the Cotter River Catchment.

Sample	$^{143}Nd/^{144}Nd$[a]	εNd (‰)	$^{87}Sr/^{86}Sr$[b]
NMG 1 0–5 cm(metased)	0.512009	−12.28	0.738097
NMG 2 0–5 cm (metased)	0.511975	−12.93	0.779228
NMG 9 BR (metased)	0.511870	−14.99	0.925066
NMG 9 0–5 cm (metased)	0.511956	−13.31	0.742813
NMG 4 0–5 cm (granodiorite)	0.512069	−11.11	0.729900
NMG 5 0–5 cm (granodiorite)	0.512131	−9.89	0.763943
NMG 6 BR (granodiorite)	0.512150	−9.52	0.740255
NMG 6 0–5 cm (granodiorite)	0.512156	−9.41	0.763537
CRC_04 3–4 cm	0.512036	−11.74	0.764717
CRC_17 16–17 cm	0.512035	−11.76	0.765407
CRC_31 30–31 cm	0.512074	−11.01	0.765186
CRC_36 35–36 cm	0.512066	−11.16	0.764505
CRC_45 44–45 cm	0.512068	−11.13	0.767512
CRC_51 50–51 cm	0.512035	−11.76	0.770539
CRC_52 51–52 cm	0.512052	−11.44	0.768907
CRC_53 52–53 cm	0.512019	−12.07	0.775228
CRC_54 53–54 cm	0.512042	−11.64	0.761164
CRC_55 54–55 cm	0.511991	−12.62	0.774975
CRC_56 55–56 cm	0.512042	−11.62	0.774534
CRC_66 65–66 cm	0.512027	−11.91	0.766303
CRC_74 73–74 cm	0.512006	−12.33	0.761705
CRC_75 74–75 cm	0.512019	−12.08	0.751846
CRC_76 75–76 cm	0.512005	−12.35	0.758113
CRC_77 76–77 cm	0.511984	−12.75	0.750446

[a] 2SE values for $^{143}Nd/^{144}Nd = \pm 0.000020$.
[b] 2SE values for $^{87}Sr/^{86}Sr = \pm 0.000053$.

soils post-fire. It has been shown that boron isotopes in the soil can have a gradient where they are isotopically heavier near the surface (attributed to biological contributions), and lighter at depth (attributed to their variable biological and lithological relative contributions; Lemarchand et al., 2012), thus suggesting that boron contributions from combusted plants would only be imparted to the top ~50 cm of soils. Though it is possible for B input from wildfires to leach to deeper depths, it is likely removed and transported away from the site during post-fire erosion shortly after the fire (Bradstock, 2008; Gómez-Rey et al., 2014). Therefore, a shallower removal of topsoil during erosion could be sufficient to transport the fire-related boron isotope signals to sediment sinks while removing the signals at the source locations. Bushfires have been shown to increase erosion by orders of magnitude (e.g. Shakesby et al., 2007). Increased erosion would likely also manifest especially prominently at our sites on topographic highs.

Finally, desorption of B from soil clays may result in the observed lack of trend with fire severity. Although experiments have shown that the adsorption of boron from combusted leaves can be partially reversible (thus displaying hysteresis), up to 100 % of adsorbed B could still be desorbed during rinsing with water (Lu et al., 2024). Studies have also found that several wetting and drying cycles may be required for boron adsorbed onto clays to display significant hysteresis (Goldberg and Suarez, 2012; Keren and O'Connor, 1982). Thus, it may be the case that a longer duration is necessary for wetting and drying cycles to "fix" any boron isotope signals of fire severity that may have been generated in our samples. Thus, we argue that hysteresis is the most likely explanation for the lack of a systemic trend of boron isotope compositions in the soil with fire severity.

The CR-01 sediments may have experienced more wetting and drying cycles during the erosion and depositional process. Therefore, positive excursions in the $\delta^{11}B$ value of the sediments may reflect the erosion and deposition of soils derived from granodiorite lithology or soils that have been derived from high-severity fires.

4.1. Sediment sources and post-fire erosion

Sr and Nd isotopes in sediments can be used in a mixed-geology catchment as a tracer for changes in source material because they are not fractionated during biological cycling or physical transport (Négrel, 2006). The Cotter River Catchment is dominated by metasedimentary bedrock in the valley bottoms and slopes, whilst granites and granodiorites predominate on the ridgelines (Nichols et al., 2006). The Nd isotope ratio of the granodiorite bedrock (0.512150 ± 0.000020) is higher than that of the metasedimentary bedrock (0.511870 ± 0.000020). However, the Sr isotope ratio of the granodiorite bedrock (0.740255 ± 0.000053) is lower than the metasedimentary bedrock

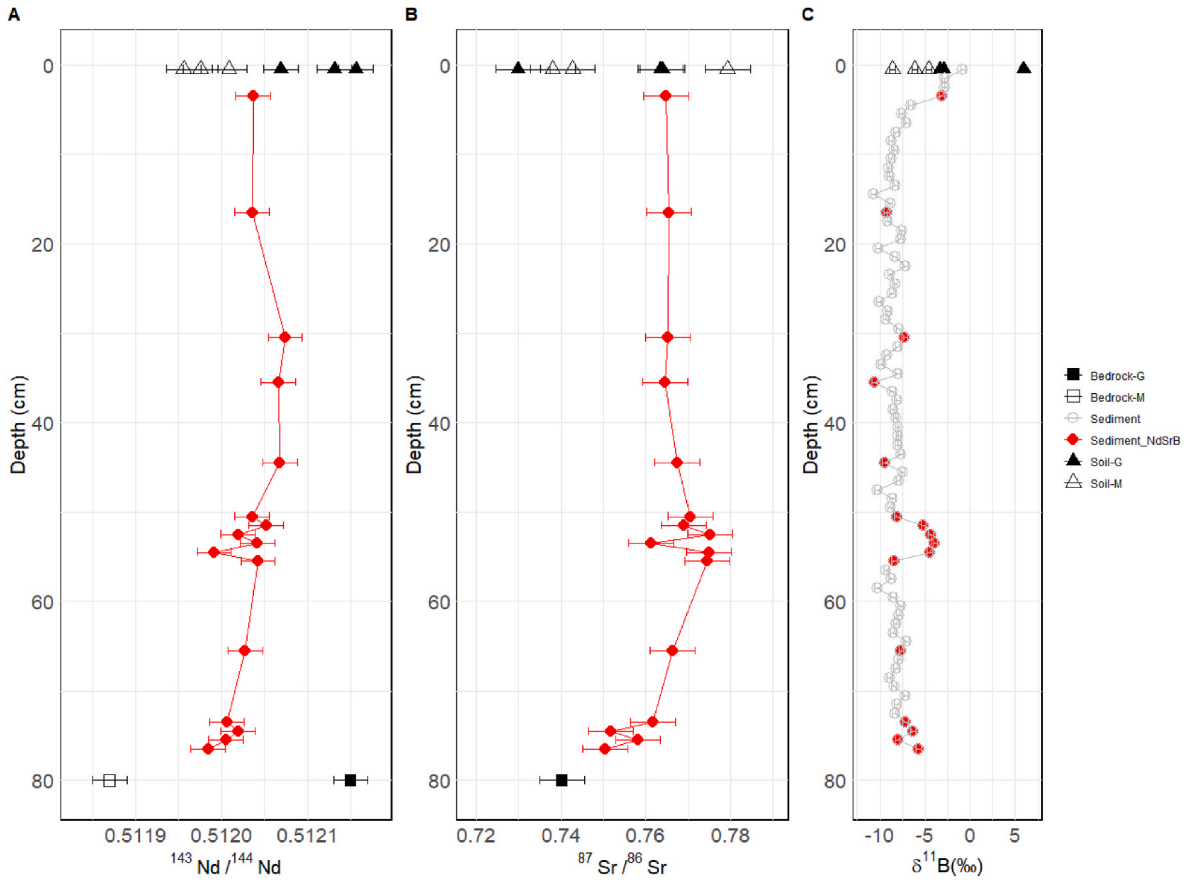

Fig. 6. A) $^{143}Nd/^{144}Nd$, B) $^{87}Sr/^{86}Sr$ ratios and C) $\delta^{11}B$ values as a function of depth in the CR-01 core sediments. The triangles represent soil samples, squares are bedrock samples, and circles are CR-01 core sediment samples. In the case of the bedrock and soil samples, closed symbols represent samples developed over the granodiorite parent material, whilst open symbols represent samples developed over the metasedimentary parent material. The $^{87}Sr/^{86}Sr$ of the metasedimentary bedrock is not graphed; however, it yielded a value of 0.925066. Red symbols represent sediment samples analysed for all three element isotopes, whilst open grey symbols were only analysed for B isotopes. The bedrock samples were not analysed for B isotopes. (For interpretation of the references to colour in this figure legend, the reader is referred to the Web version of this article.)

(0.925066 ± 0.000053). This is in agreement with Healy et al. (2004), where the authors found that S-type granites in the Lachlan Fold Belt (such as the granodiorites in the Cotter Catchment) had higher $^{143}Nd/^{144}Nd$ ratios and lower $^{87}Sr/^{86}Sr$ ratios compared to metasedimentary rocks. The relationship between the Sr and Nd isotope ratios of soil samples, however, is more complex. The soils developed on metasedimentary parent material have higher Nd and lower Sr ratios than the bedrock values. However, this trend is not apparent for the soils developed on granodiorite parent material. The Nd isotope ratio shows no systematic relationship with fire severity for soils developed on either bedrock type. However, the Sr isotope ratios show opposing trends depending on the bedrock type. Soils developed over metasedimentary parent material that burnt at extreme severity during the 2019–20 fires showed higher Sr isotope ratio values, while low-severity fires showed a lower Sr isotope ratio. Conversely, soils that burnt at extreme severity in 2019–20 and formed over granodiorite bedrock showed lower Sr ratio values and soils burnt at low severity showed higher Sr isotope ratio values. This trend could have been affected by the larger error for the Sr ratio values. Previous studies have largely analysed changes in Sr concentration following fire, finding an increase compared to unburnt soils hypothesised to occur from the bonding of Sr to carbonates (Natali et al., 2023; Shapchenkova et al., 2024). However, at present, there are no existing studies that analyse changes in Sr isotopic fractionation with different fire severity.

Over the top ~45 cm, the Nd isotope ratio values of the CR-01 sediments are between the ranges for the soils developed over the two bedrock types, suggesting the mixing of soils from the two parent materials. Below ~45 cm, the Nd isotope ratio trends towards the metasedimentary bedrock, more typical of the valleys and tributaries of the Cotter River. This trend is not reflected in the Sr isotope ratio values, however, due to the overlap in the ranges for soils developed over the two bedrock types. Whilst a mass balance is not possible as Sr and Nd concentrations were not measured, comparison with the B isotope composition of sediments reflects that of the soils, where there is a large overlap in the $\delta^{11}B$ values recorded for the soils and sediments. The B isotope ratios of the sediment samples suggest that the sediments are largely derived from metasedimentary bedrock. This is not unexpected, given the location of the CR-01 site on the floodplain of the Cotter River, which is dominated by metasedimentary bedrock, suggesting the predominance of sediment deposition from the valley bottoms and slopes. Assuming that positive excursions of $\delta^{11}B$ in the CR-01 core reflect an increased deposition of soils formed over granodiorite bedrock, this suggests that the peak at 51–55 cm reflects a possible increase in erosion and deposition of soils from the ridgelines where granodiorite predominates. However, this trend is not reflected in the Sr and Nd isotope ratios. Whilst this may be the result of poorer quality control for Sr and Nd results, it is more likely that the B isotope ratios do not solely reflect the lithology of the soil's parent material but also the organic matter contributions, which can be used as a proxy for past fire events.

The Sr and Nd ratios with depth suggest no major changes in source over the last ~3000 years recorded in the CR-01 sediments. Between 30 and 80 cm depth, there is an increase in the Nd isotope ratio, which could suggest increased deposition of soils developed over the granodiorite bedrock. However, this should be associated with a decrease in

the Sr isotope ratio, which is not shown in the core sediments. Between 0 and 30 cm depth, the Nd isotope ratio decreases, suggesting a larger input from soils developed over metasedimentary bedrock, but due to the overlap in the Sr isotope ratios for soils developed from the two bedrock types, this trend is not observed.

4.2. Fire severity and intensity changes through time

Carbon and N concentrations are highest in the top ~25 cm of the core, corresponding to the last ~200–300 years of sediment deposition (Fig. 3 and Supplementary Fig. 2). Below ~30 cm, C and N concentrations are relatively constant and low (<1 wt% and <0.15 % for C and N contents, respectively) (Fig. 3 and Supplementary Fig. 2). Changes in C and N concentrations, and the C/N ratios, with depth do not correlate with changes in the aromatic/aliphatic ratio. The aromatic/aliphatic ratio of CR-01 sediments has been used, in combination with that of swamp sediments in the Blue Mountains of NSW, to suggest an increase in the frequency of high-intensity fires in the last 200 years compared to the previous 3000 years (Ryan et al., 2024). By comparing the changes in the aromatic/aliphatic ratio with existing palaeoclimate records, we hypothesised that this increase was the result of complex interactions between climate, vegetation and people (Ryan et al., 2024). Prolonged drought events were also shown to increase over a similar period, increasing the incidence of anthropogenic-ignited fire events coinciding with extreme fire weather (Bradstock, 2008; Palmer et al., 2023; Seydack et al., 2007). The expansion of eucalypt species since British colonisation has also promoted fire spread and higher fire temperatures (Hope, 2006; Hope and Clark, 2008; Younes et al., 2024). The lack of correlation between fire-affected sediments, as identified by the aromatic/aliphatic ratio, and the concentrations of C and N may be due to the poor preservation of the fire signature over the duration of the record.

Previous studies have shown a complex relationship between fire, the C/N ratio, and concentrations of both C and N. Some studies have found an increase in the C/N ratio, possibly due to N mobilisation and reduced microbial decomposition (Krull et al., 2004; Schmidt and Noack, 2000), whilst others find a decrease in the C/N ratio as a result of increased C volatilisation, thus decreasing the flux of C to lake sediments (Wu and Porinchu, 2020; Zaccone et al., 2014). Reduced C content has been shown to take up to two years to return to pre-fire stores (Martín et al., 2012); however, no change in C content has also been shown, hypothesised to result from C replenishment through post-fire litterfall (Nave et al., 2011). Thus, the complex response of C and N concentrations to fire, along with the possibility of restoration to pre-fire concentrations within ≤2 years, suggests a possible explanation for the lack of relationship with fire-affected layers, as recorded by the aromatic/aliphatic ratio.

It has been hypothesised that following a high-severity fire, soils are characterised by higher $\delta^{11}B$ values compared to soils that have been exposed to low-severity fire or no fire, due to the incorporation of B into soil clays from ashed leaf material from tree canopies, enriched in ^{11}B (Lu et al., 2022, 2024). Lu et al. (2024) found that when rainwater reacted with combusted eucalyptus leaves, the $\delta^{11}B$ value of the rainwater increased to ~29 ‰, equivalent to unburnt leaves. The desorption of B from ash into the leaching solution was shown to occur without fractionation, and the B content of the leaching solution increased with higher temperatures (Lu et al., 2024). Therefore, following a fire of high intensity and severity and a subsequent rainfall event, B is desorbed from ash and mobilised in the groundwater and streamwater where it can be adsorbed by clays. Ryan et al. (2023) showed that this isotopic signal may be transferred to sediment deposits, where sediments displaying higher $\delta^{11}B$ values may reflect past high-severity fire events. In CR-01 core sediments, $\delta^{11}B$ values decrease with increasing depth in the top ~10 cm. Previous studies have made similar observations where higher values near the surface were explained by vegetation and atmospheric inputs (Ercolani et al., 2019; Roux et al., 2022). Therefore, despite the associated increase in the aromatic/aliphatic ratio at the surface of the CR-01 core, higher $\delta^{11}B$ values in the top 4 cm may not reflect a past fire event, but rather vegetation and atmospheric inputs of B into the sediment deposit.

At 51–55 cm, corresponding to an age of 1408 (+94/–114)–1516 (+126/–116) cal yr BP, a higher $\delta^{11}B$ value may suggest a past high-severity fire event (Fig. 4C). Worthy (2013) identified a possible fire-related sedimentation event at 1280 ± 100 cal yr BP in the Cotter River Catchment, which is within error. Eriksson et al. (2006) and Hope and Clark (2008) also observed increased coarse-grained material and catchment incision in neighbouring catchments at ~1300 and 1317 ± 135 cal yr BP, respectively, postulated to be associated with a fire-induced erosion event. Sediment records from Club Lake, an alpine lake ~200 km from the CR-01 site, suggest that the period from 1600 to 1000 cal yr BP was a warming period, characterised by increased charcoal and an expansion of *Eucalyptus* sub-alpine woodland and a reduction in alpine species (Thomas et al., 2022). Therefore, this warming period could have increased the occurrence of suitable fire-weather conditions, accounting for the fire-related erosion events recorded by Worthy (2013), Eriksson et al. (2006) and Hope and Clark (2008) and the possible high-severity fire suggested by the high $\delta^{11}B$ values.

Interestingly, the higher $\delta^{11}B$ value at 51–55 cm (interpreted as a high-severity fire) is not associated with a high aromatic/aliphatic ratio. This is unexpected, as a high-severity fire should produce temperatures high enough to increase the aromatic/aliphatic ratio of sediments, as previously observed (Ryan et al., 2023). It is not clear why this hypothesised fire event is not recorded in the FTIR spectra.

Several negative $\delta^{11}B$ excursions are observed at 14–15 cm, 20–21 cm, 26–27 cm, 33–34 cm, 35–36 cm, 44–45 cm, 47–48 cm and 58–59 cm depth. Lu et al. (2022) showed that the clay fractions of soils that had experienced consecutive low-severity fires had a lower $\delta^{11}B$ value compared to sites that had experienced a high-severity fire because burning of bark imparts lower $\delta^{11}B$ values to soil than burning of leaves. This suggests that the negative excursions in the CR-01 core may record low-severity fire events. The negative $\delta^{11}B$ excursions at 14–15 cm, 20–21 cm, 33–34 cm, and 44–45 cm coincide with or are 1 cm offset from positive peaks in the aromatic/aliphatic ratio at 11–16 cm, 19–20 cm, 33–34 cm and 45–46 cm, respectively. This suggests that these lower-severity fires may have recorded temperatures high enough (>250 °C) to significantly increase the aromatic/aliphatic ratio of sediments (Araya et al., 2017; Guo and Bustin, 1998). This is not plausible in the Australian context due to the predominance of eucalypt species, resulting in high-intensity fires that always consume the canopy (i.e. high-severity fires) (Bradstock et al., 2010; Collins et al., 2014). Alternatively, increased aromatic/aliphatic ratios can result from prolonged heating duration, where during typical fire events, temperatures >250 °C are only sustained for ~40 min (Doerr et al., 2004; Raison et al., 1986). The exception to this is during smouldering combustion or where large accumulations of organic matter are consumed (Doerr et al., 2004). Under these conditions, the most significant effects are observed in the first 2–3 h (Aldeias et al., 2016). Thus, the association of low $\delta^{11}B$ values with high aromatic/aliphatic ratios could be explained by low-severity fires, where vegetation was burned for ~40 min.

5. Conclusion

We aimed to assess how the C and N contents, FTIR spectra and B isotope ratio of sediment deposits record past fire characteristics in Namadgi National Park in southeastern Australia. By applying FTIR spectroscopy and B isotopes to sediments, we provide a ~3000-year record of past fire intensity and severity in Namadgi National Park in southeastern Australia. The aromatic/aliphatic ratio showed increased fire frequency and intensity over the last ~200 years compared to the previous 3000 years. Strontium and Nd isotope ratios suggest that there has been no significant change in sediment source in the CR-01

catchment over the last ~3000 years and that the positive peaks in the B isotope ratio of sediments were the result of both lithology and organic matter contributions from fires. This was particularly due to combusted leaves, which are enriched in the heavier isotope, suggesting higher fire severity. For some fires recorded by both proxies, negative excursions in the B isotope ratio coincided with positive excursions in the aromatic/aliphatic ratio, suggesting that lower-severity fires burning for prolonged heating durations may have resulted in higher contributions from burned bark. The C and N content and C/N ratio showed no consistent relationship with fire events, suggesting that these parameters are less effective for identifying past fire events in this landscape. Our results vitally inform management through improved understanding of past changes and extend the hindcasting capacity of mechanistic models to inform future management strategies under the influence of climate change.

Author contributions

Rebecca Ryan: Conceptualization, Formal analysis, Investigation, Methodology, Writing - Original Draft, Visualization; Shawn Lu: Investigation, Visualization, Writing – review and editing; Damien Lemarchand: Funding acquisition, Methodology, Writing – review and editing; Zoë Thomas: Methodology, Formal analysis, Supervision, Writing – review and editing; Ivan Simkovic: Investigation; Pavel Dlapa: Methodology, Writing – review and editing; Martin Worthy: Investigation; Robert Wasson: Writing – review and editing; Ross Bradstock: Funding acquisition, Writing – review and editing; Katharine Haynes: Supervision, Writing – review and editing and Anthony Dosseto: Conceptualization, Funding acquisition, Project administration, Supervision, Writing – review and editing.

Funding

Funding was provided by ARC Discovery Grant DP200101123. Support from the grant SGA VEGA 1/0703/23 is also appreciated.

Declaration of competing interest

The authors declare that they have no known competing financial interests or personal relationships that could have appeared to influence the work reported in this paper.

Acknowledgements

We would like to thank ACT Parks for permitting site access and sample collection. Funding was provided by ARC Discovery Grant DP200101123. Support from the grant SGA VEGA 1/0703/23 is also appreciated. RR acknowledges an APA PhD scholarship and a top-up scholarship from Natural Hazards Research Australia.

Appendix A. Supplementary data

Supplementary data to this article can be found online at https://doi.org/10.1016/j.quascirev.2025.109605.

Data availability

All data and/or code is contained within the submission.

References

Abakumov, E., Maksimova, E., Tsibart, A., 2018. Assessment of postfire soils degradation dynamics : stability and molecular composition of humic acids with use of spectroscopy methods. Land Degrad. Dev. 2092–2101. https://doi.org/10.1002/ldr.2872.

Aldeias, V., Dibble, H.L., Sandgathe, D., Goldberg, P., McPherron, S.J.P., 2016. How heat alters underlying deposits and implications for archaeological fire features: a controlled experiment. J. Archaeol. Sci. 67, 64–79. https://doi.org/10.1016/j.jas.2016.01.016.

Araya, S.N., Fogel, M.L., Berhe, A.A., 2017. Thermal alteration of soil organic matter properties: a systematic study to infer response of Sierra Nevada climosequence soils to forest fires. Soils 3, 31–44. https://doi.org/10.5194/soil-3-31-2017.

Baek, S.-J., Park, A., Ahn, Y.-J., Choo, J., 2015. Baseline correction using asymmetrically reweighted penalized least squares smoothing. Analyst 140, 250–257. https://doi.org/10.1039/c4an01061b.

Beasley, M.M., Bartelink, E.J., Taylor, L., Miller, R.M., 2014. Comparison of transmission FTIR, ATR, and DRIFT spectra: implications for assessment of bone bioapatite diagenesis. J. Archaeol. Sci. 46, 16–22. https://doi.org/10.1016/j.jas.2014.03.008.

Berna, F., Behar, A., Shahack-Gross, R., Berg, J., Boaretto, E., Gilboa, A., Sharon, I., Shalev, S., Shilstein, S., Yahalom-Mack, N., Zorn, J.R., Weiner, S., 2007. Sediments exposed to high temperatures: reconstructing pyrotechnological processes in late Bronze and Iron Age Strata at Tel Dor (Israel). J. Archaeol. Sci. 34, 358–373. https://doi.org/10.1016/j.jas.2006.05.011.

Blevins, D.G., Lukaszewski, K.M., 1998. Boron IN plant STRUCTURE and function. Annu. Rev. Plant Physiol. Plant Mol. Biol. 49, 481–500. https://doi.org/10.1146/annurev.arplant.49.1.481.

Bowman, D.M.J.S., Murphy, B.P., Neyland, D.L.J., Williamson, G.J., Prior, L.D., 2014. Abrupt fire regime change may cause landscape-wide loss of mature obligate seeder forests. Glob. Change Biol. 20, 1008–1015. https://doi.org/10.1111/gcb.12433.

Bradstock, R.A., 2008. Effects of large fires on biodiversity in south-eastern Australia: disaster or template for diversity? Int. J. Wildland Fire 17, 809–822. https://doi.org/10.1071/WF07153.

Bradstock, R.A., Hammill, K.A., Collins, L., Price, O., 2010. Effects of weather, fuel and terrain on fire severity in topographically diverse landscapes of south-eastern Australia. Landsc. Ecol. 25, 607–619. https://doi.org/10.1007/s10980-009-9443-8.

Bronk Ramsey, C., 2009. Dealing with outliers and offsets in radiocarbon dating. Radiocarbon 51, 1023–1045. https://doi.org/10.1017/s0033822200034093.

Carey, Evans, Hann, Lintermans, 2003. Wildfires in the ACT 2003: report on initial impacts on natural ecosystems. Environment ACT Canberra.

Chafer, C.J., 2008. A comparison of fire severity measures: an Australian example and implications for predicting major areas of soil erosion. Catena 74, 235–245. https://doi.org/10.1016/j.catena.2007.12.005.

Chetelat, B., Gaillardet, J., Chen, J. Bin, 2021. Dynamic of boron in forest ecosystems traced by its isotopes: a modeling approach. Chem. Geol. 560, 1–13. https://doi.org/10.1016/j.chemgeo.2020.119994.

Chuvieco, E., Congalton, R.G., 1989. Application of remote sensing and geographic information systems to Forest hazard mapping. Remote Sens. Environ. 159, 147–159.

Cividini, D., Lemarchand, D., Chabaux, F., Boutin, R., Pierret, M., 2010. From biological to lithological control of the B geochemical cycle in a forest watershed (Strengbach , Vosges). Geochem. Cosmochim. Acta 74, 3143–3163. https://doi.org/10.1016/j.gca.2010.03.002.

Clark, J.S., 1988. Particle motion and the theory of charcoal analysis: source area, transport, deposition, and sampling. Quat. Res. 30, 67–80. https://doi.org/10.1016/0033-5894(88)90088-9.

Clarke, P.J., Knox, K.J.E., Bradstock, R.A., Munoz-Robles, C., Kumar, L., 2014. Vegetation, terrain and fire history shape the impact of extreme weather on fire severity and ecosystem response. J. Veg. Sci. 25, 1033–1044. https://doi.org/10.1111/jvs.12166.

Collins, L., Bradstock, R.A., Clarke, H., Clarke, M.F., Nolan, R.H., Penman, T.D., 2021. The 2019/2020 mega-fires exposed Australian ecosystems to an unprecedented extent of high-severity fire. Environ. Res. Lett. 16. https://doi.org/10.1088/1748-9326/abeb9e.

Collins, L., Bradstock, R.A., Penman, T.D., 2014. Can precipitation influence landscape controls on wildfire severity' A case study within temperate eucalypt forests of south-eastern Australia. Int. J. Wildland Fire 23, 9–20. https://doi.org/10.1071/WF12184.

Constantine IV, M., Mooney, S., Hibbert, B., Marjo, C., Bird, M., Cohen, T., Forbes, M., McBeath, A., Rich, A., Stride, J., 2021. Using charcoal, ATR FTIR and chemometrics to model the intensity of pyrolysis: exploratory steps towards characterising fire events. Sci. Total Environ. 783, 147052. https://doi.org/10.1016/j.scitotenv.2021.147052.

Constantine IV, M., Williams, A.N., Francke, A., Cadd, H., Forbes, M., Cohen, T.J., Zhu, X., Mooney, S.D., 2023a. Exploration of the burning question : a long history of fire in Eastern Australia with and without people. Fire 6, 4–13.

Constantine IV, M., Zhu, X., Cadd, H., Mooney, S., 2023b. Investigating the effect of oxidants on the quantification and characterization of charcoal in two Southeast Australian sedimentary records. Fire 6, 4–13. https://doi.org/10.3390/fire6020054.

Daniell, T., White, I., 2005. Bushfires and their implications for management of future water supplies in the Australian Capital Territory. Clim. Anthropog. Impacts Var. Water Resour. 22–24.

de Santana, H., Toni, L.R.M., Benetoli, L.O.d.B., Zaia, C.T.B.V., Rosa, M., Zaia, D.A.M., 2006. Effect in glyphosate adsorption on clays and soils heated and characterization by FT-IR spectroscopy. Geoderma 136, 738–750. https://doi.org/10.1016/j.geoderma.2006.05.012.

Dixon, K.M., Cary, G.J., Worboys, G.L., Seddon, J., Gibbons, P., 2018. A comparison of fuel hazard in recently burned and long-unburned forests and woodlands. Int. J. Wildland Fire 27, 609–622.

Dlapa, P., Bodí, M.B., Mataix-solera, J., Cerdà, A., Doerr, S.H., 2013. FT-IR spectroscopy reveals that ash water repellency is highly dependent on ash chemical composition. Catena 108, 35–43. https://doi.org/10.1016/j.catena.2012.02.011.

Doerr, S.H., Blake, W.H., Shakesby, R.A., Stagnitti, F., Vuurens, S.H., Humphreys, G.S., Wallbrink, P., 2004. Heating effects on water repellency in Australian eucalypt forest

soils and their value in estimating wildfire soil temperatures. Int. J. Wildland Fire 13, 157–163. https://doi.org/10.1071/WF03051.
Driscoll, D.A., Macdonald, K.J., Gibson, R.K., Doherty, T.S., Nimmo, D.G., Nolan, R.H., Ritchie, E.G., Williamson, G.J., Heard, G.W., Tasker, E.M., Bilney, R., Porch, N., Collett, R.A., Crates, R.A., Hewitt, A.C., Pendall, E., Boer, M.M., Gates, J., Boulton, R. L., Mclean, C.M., Groffen, H., Maisey, A.C., Beranek, C.T., Ryan, S.A., Callen, A., Hamer, A.J., Stauber, A., Daly, G.J., Gould, J., Klop-Toker, K.L., Mahony, M.J., Kelly, O.W., Wallace, S.L., Stock, S.E., Weston, C.J., Volkova, L., Black, D., Gibb, H., Grubb, J.J., McGeoch, M.A., Murphy, N.P., Lee, J.S., Dickman, C.R., Neldner, V.J., Ngugi, M.R., Miritis, V., Köhler, F., Perri, M., Denham, A.J., Mackenzie, B.D.E., Reid, C.A.M., Rayment, J.T., Arriaga-Jiménez, A., Hewins, M.W., Hicks, A., Melbourne, B.A., Davies, K.F., Bitters, M.E., Linley, G.D., Greenville, A.C., Webb, J. K., Roberts, B., Letnic, M., Price, O.F., Walker, Z.C., Murray, B.R., Verhoeven, E.M., Thomsen, A.M., Keith, D., Lemmon, J.S., Ooi, M.K.J., Allen, V.L., Decker, O.T., Green, P.T., Moussalli, A., Foon, J.K., Bryant, D.B., Walker, K.L., Bruce, M.J., Madani, G., Tscharke, J.L., Wagner, B., Nitschke, C.R., Gosper, C.R., Yates, C.J., Dillon, R., Barrett, S., Spencer, E.E., Wardle, G.M., Newsome, T.M., Pulsford, S.A., Singh, A., Roff, A., Marsh, K.J., Mcdonald, K., Howell, L.G., Lane, M.R., Cristescu, R. H., Witt, R.R., Cook, E.J., Grant, F., Law, B.S., Seddon, J., Berris, K.K., Shofner, R.M., Barth, M., Welz, T., Foster, A., Hancock, D., Beitzel, M., Tan, L.X.L., Waddell, N.A., Fallow, P.M., Schweickle, L., Le Breton, T.D., Dunne, C., Green, M., Gilpin, A.M., Cook, J.M., Power, S.A., Hogendoorn, K., Brawata, R., Jolly, C.J., Tozer, M., Reiter, N., Phillips, R.D., 2024. Biodiversity impacts of the 2019–2020 Australian megafires. Nature 34. https://doi.org/10.1038/s41586-024-08174-6.
Ellerbrock, R., Gerke, H.H., Bachmann, J., Goebel, M.-O., 2005. Composition of organic matter fractions for explaining wettability of three Forest soils. Soil Sci. Soc. Am. J. 69, 57.
Ercolani, C., Lemarchand, D., Dosseto, A., 2019. Insights on catchment-wide weathering regimes from boron isotopes in riverine material. Geochem. Cosmochim. Acta 261, 35–55. https://doi.org/10.1016/j.gca.2019.07.002.
Eriksson, M.G., Olley, J.M., Kilham, D.R., Pietsch, T., Wasson, R.J., 2006. Aggradation and incision since the very late Pleistocene in the Naas River, south-eastern Australia. Geomorphology 81, 66–88. https://doi.org/10.1016/j.geomorph.2006.04.001.
Gangjian, W., Jingxian, W., Ying, L., Ting, K., Zhongyuan, R., Jinlonga, M., Yigang, X., 2013. Measurement on high-precision boron isotope of silicate materials by a single column purification. J. Anal. At. Spectrom 28, 606–612. https://doi.org/10.1039/c3ja30333k.
Gibson, R., Danaher, T., Hehir, W., Collins, L., 2020. A remote sensing approach to mapping fire severity in south-eastern Australia using sentinel 2 and random forest. Remote Sens. Environ. 240, 111702. https://doi.org/10.1016/j.rse.2020.111702.
Goldberg, S., Corwin, D.L., Shouse, P.J., Suarez, D.L., 2005. Prediction of boron adsorption by field samples of diverse textures. https://doi.org/10.2136/sssaj2004.0354.
Goldberg, S., Suarez, D.L., 2012. Role of organic matter on boron adsorption-desorption hysteresis of soils. Soil Sci. 177, 417–423. https://doi.org/10.1097/SS.0b013e318256bc0c.
Gómez-Rey, M.X., García-Marco, S., Fernández, C., Couto-Vázquez, A., González-Prieto, S.J., 2014. Effects of post-fire soil stabilisation techniques on trace elements lost by erosion. Int. J. Wildland Fire 23, 93–103.
Gosling, W.D., Cornelissen, H.L., McMichael, C.N.H., 2019. Reconstructing past fire temperatures from ancient charcoal material. Palaeogeogr. Palaeoclimatol. Palaeoecol. 520, 128–137. https://doi.org/10.1016/j.palaeo.2019.01.029.
Granged, A.J.P., Jordán, A., Zavala, L.M., Muñoz-Rojas, M., Mataix-Solera, J., 2011. Short-term effects of experimental fire for a soil under eucalyptus forest (SE Australia). Geoderma 167–168, 125–134. https://doi.org/10.1016/j.geoderma.2011.09.011.
Griffiths, P., 1990. Fourier transform infrared spectrometry. Science 222, 297–302.
Guo, Y., Bustin, R.M., 1998. FTIR spectroscopy and reflectance of modern charcoals and fungal decayed woods : implications for studies of inertinite in coals. Int. J. Coal Geol. 37, 29–53.
Hammill, K.A., Bradstock, R.A., 2006. Remote sensing of fire severity in the Blue Mountains: influence of vegetation type and inferring fire intensity. Int. J. Wildland Fire 15, 213–226. https://doi.org/10.1071/WF05051.
Healy, B., Collins, W.J., Richards, S.W., 2004. A hybrid origin for Lachlan S-type granites: the Murrumbidgee Batholith example. Lithos 78, 197–216. https://doi.org/10.1016/j.lithos.2004.04.047.
Hennebelle, A., Aleman, J.C., Ali, A.A., Bergeron, Y., Carcaillet, C., Grondin, P., Landry, J., Blarquez, O., 2020. The reconstruction of burned area and fire severity using charcoal from boreal lake sediments. Holocene 30, 1400–1409. https://doi.org/10.1177/0959683620932979.
Hogg, A.G., Heaton, T.J., Hua, Q., Palmer, J.G., Turney, C.S.M., Southon, J., Bayliss, A., Blackwell, P.G., Boswijk, G., Bronk Ramsey, C., Pearson, C., Petchey, F., Reimer, P., Reimer, R., Wacker, L., 2020. SHCal20 Southern Hemisphere Calibration, 0-55,000 Years cal BP. Radiocarbon 62, 759–778. https://doi.org/10.1017/RDC.2020.59.
Hong, H., Chen, S., Fang, Q., Algeo, T.J., Zhao, L., 2019. Adsorption of organic matter on clay minerals in the Dajiuhu peat soil chronosequence, South China. Appl. Clay Sci. 178, 105125. https://doi.org/10.1016/j.clay.2019.105125.
Hope, G., 2006. Histories of wetlands in the Australian Capital Territory and the bog recovery program. In: National Parks Association ACT Symposium 2006: Caring for Namadgi – Science and People, pp. 131–143.
Hope, G., Clark, R., 2008. A tale of two swamps: Sub-Alpine peatlands in the Kelly-Scabby area of Namadgi National Park. In: NPA ACT Symposium 2008: Corridors for Survival in a Changing World, pp. 61–73.
Hua, Q., Turnbull, J.C., Santos, G.M., Rakowski, A.Z., Ancapichún, S., De Pol-Holz, R., Hammer, S., Lehman, S.J., Levin, I., Miller, J.B., Palmer, J.G., Turney, C.S.M., 2021. Atmospheric radiocarbon for the period 1950-2019. Radiocarbon 64, 1–23. https://doi.org/10.1017/RDC.2021.95.
Jacobsen, S.B., Wasserburg, G.J., 1980. Sm-Nd isotopic evolution of chondrites. Earth Planet Sci. Lett. 50, 139–155.
Jweda, J., Bolge, L., Class, C., Goldstein, S.L., 2016. High precision sr-nd-hf-pb isotopic compositions of USGS reference material BCR-2. Geostand. Geoanalytical Res. 40, 101–115. https://doi.org/10.1111/j.1751-908X.2015.00342.x.
Keeley, J.E., 2009. Fire intensity, fire severity and burn severity: a brief review and suggested usage. Int. J. Wildland Fire 18, 116–126. https://doi.org/10.1071/WF07049.
Keiluweit, M., Nico, P.S., Johnson, M., Kleber, M., 2010. Dynamic molecular structure of plant biomass-derived black carbon (biochar). Environ. Sci. Technol. 44, 1247–1253. https://doi.org/10.1021/es9031419.
Keren, R., O'Connor, G.A., 1982. Effect of exchangeable ions and ionic strength on boron adsorption by montmorillonite and illite. Clays Clay Miner. 30, 341–346. https://doi.org/10.1346/ccmn.1982.0300504.
Killick, R., Eckley, I.A., 2014. Changepoint: an R package for changepoint analysis. J. Stat. Software 3, 1–19. https://doi.org/10.18637/jss.v058.i03.
Krull, E.S., Thompson, C.H., Skjemstad, J.O., 2004. Chemistry, radiocarbon ages, and development of a subtropical acid peat in Queensland, Australia. Aust. J. Soil Res. 42, 411–425. https://doi.org/10.1071/SR03144.
Le Losq, C., 2018. Rampy: a Python library for processing spectroscopic (IR, Raman. XAS… data. Zenodo.
Leigh, C., Bush, A., Harrison, E.T., Ho, S.S., Luke, L., Rolls, R.J., Ledger, M.E., 2015. Ecological effects of extreme climatic events on riverine ecosystems: insights from Australia. Freshw. Biol. 60, 2620–2638. https://doi.org/10.1111/fwb.12515.
Lemarchand, D., Cividini, D., Turpault, M., Chabaux, F., 2012. Boron isotopes in different grain size fractions : exploring past and present water – rock interactions from two soil profiles (Strengbach , Vosges Mountains). Geochem. Cosmochim. Acta 98, 78–93. https://doi.org/10.1016/j.gca.2012.09.009.
Lu, S., Dosseto, A., Lemarchand, D., 2024. Boron in wildfires : new insights into boron isotope fractionation during volatilisation, leaching and adsorption after combustion. Geochem. Cosmochim. Acta 379, 208–218.
Lu, S., Dosseto, A., Lemarchand, D., Dlapa, P., Simkovic, I., Bradstock, R., 2022. Investigating boron isotopes and FTIR as proxies for bushfire severity. Catena, 106621. https://doi.org/10.1016/j.catena.2022.106621, 1–15.
Madejová, J., Komadel, P., 2001. Baseline studies of the clay Minerals Society source clays: infrared methods. Clays Clay Miner. 49, 410–432.
Maezumi, S.Y., Gosling, W.D., Kirschner, J., Chevalier, M., Cornelissen, H.L., Heinecke, T., McMichael, C.N.H., 2021. A modern analogue matching approach to characterize fire temperatures and plant species from charcoal. Palaeogeogr. Palaeoclimatol. Palaeoecol. 578, 110580. https://doi.org/10.1016/j.palaeo.2021.110580.
Malone, S.L., Kobziar, L.N., Staudhammer, C.L., Abd-Elrahman, A., 2011. Modeling relationships among 217 fires using remote sensing of burn severity in southern pine forests. Remote Sens. 3, 2005–2028. https://doi.org/10.3390/rs3092005.
Martín, A., Díaz-Raviña, M., Carballas, T., 2012. Short- and medium-term evolution of soil properties in Atlantic forest ecosystems affected by wildfires. Land Degrad. Dev. 23, 427–439. https://doi.org/10.1002/ldr.1078.
Mateo, P., Bonilla, I., Fernández-Valiente, E., Sanchez-Maeso, E., 1986. Essentiality of boron for dinitrogen fixation in Anabaena sp. PCC 7119. Plant Physiol. 81, 430–433. https://doi.org/10.1104/pp.81.2.430.
McLauchlan, K.K., Higuera, P.E., Miesel, J., Rogers, B.M., Schweitzer, J., Shuman, J.K., Tepley, A.J., Varner, J.M., Veblen, T.T., Adalsteinsson, S.A., Balch, J.K., Baker, P., Batllori, E., Bigio, E., Brando, P., Cattau, M., Chipman, M.L., Coen, J., Crandall, R., Daniels, L., Enright, N., Gross, W.S., Harvey, B.J., Hatten, J.A., Hermann, S., Hewitt, R.E., Kobziar, L.N., Landesmann, J.B., Loranty, M.M., Maezumi, S.Y., Mearns, L., Moritz, M., Myers, J.A., Pausas, J.G., Pellegrini, A.F.A., Platt, W.J., Roozeboom, J., Safford, H., Santos, F., Scheller, R.M., Sherriff, R.L., Smith, K.G., Smith, M.D., Watts, A.C., 2020. Fire as a fundamental ecological process: research advances and frontiers. J. Ecol. 108, 2047–2069. https://doi.org/10.1111/1365-2745.13403.
Mooney, S.D., Tinner, W., 2011. The analysis of charcoal in peat and organic sediments. Mires Peat 7, 1–18.
Natali, C., Ferrari, M., Bragagni, A., Bianchini, G., Salani, G.M., Avanzinelli, R., Ghiotto, M., 2023. The trace element distribution in peat soils affected by natural burning events: a proxy of the original composition and metals mobility assessment. Sci. Total Environ. 905, 167826. https://doi.org/10.1016/j.scitotenv.2023.167826.
Nave, L.E., Vance, E.D., Swanston, C.W., 2011. Fire effects on temperate forest soil C and N storage. Ecol. Appl. 21, 1189–1201.
Négrel, P., 2006. Water-granite interaction: clues from strontium, neodymium and rare earth elements in soil and waters. Appl. Geochem. 21, 1432–1454. https://doi.org/10.1016/j.apgeochem.2006.04.007.
Nichols, S., Norris, R., Maher, W., Thoms, M., 2006. Ecological effects of serial impoundment on the Cotter River, Australia. Hydrobiologia 572, 255–273. https://doi.org/10.1007/s10750-005-0995-6.
Nolan, R.H., Bowman, D.M.J.S., Clarke, H., Haynes, K., Ooi, M.K.J., Price, O.F., Williamson, G.J., Whittaker, J., Bedward, M., Boer, M.M., Cavanagh, V.I., Collins, L., Gibson, R.K., Griebel, A., Jenkins, M.E., Keith, D.A., McIlwee, A.P., Penman, T.D., Samson, S.A., Tozer, M.G., Bradstock, R.A., 2021a. What do the australian black summer fires signify for the global fire crisis? Fire 4. https://doi.org/10.3390/fire4040097.
Nolan, R.H., Collins, L., Leigh, A., Ooi, M.K.J., Curran, T.J., Fairman, T.A., Resco de Dios, V., Bradstock, R., 2021b. Limits to post-fire vegetation recovery under climate change. Plant Cell Environ. 44, 3471–3489. https://doi.org/10.1111/pce.14176.

Palmer, J.G., Verdon-Kidd, D., Allen, K.J., Higgins, P., Cook, B.I., Cook, E.R., Turney, C.S. M., Baker, P.J., 2023. Drought and deluge: the recurrence of hydroclimate extremes during the past 600 years in eastern Australia's Natural Resource Management (NRM) clusters. Nat. Hazards. https://doi.org/10.1007/s11069-023-06288-0.

Park, H., Schlesinger, W.H., 2002. Global biogeochemical cycle of boron. Glob. Biogeochem. Cycles 16. https://doi.org/10.1029/2001gb001766, 20-1-20–11.

Prescott, J.R., Hutton, J.T., 1994. Cosmic ray contributions to dose rates for luminescence and ESR dating: large depths and long term time variations. Radiat. Meas. 23, 497–500.

Pryor, L.D., 1939. The Bush fire problem in the Australian Capital Territory. Aust. For. 4, 33–38.

Raison, R.J., Woods, P.V., Jakobsen, B.F., Bary, G.A.V., 1986. Soil temperatures during and following low-intensity prescribed burning in a Eucalyptus pauciflora Forest. Aust. J. Soil Res. 24, 33–47.

Ramsey, B., 2006. New approaches to constructing age models : OxCal4. PAGES News 14, 14–15.

Rausa, R., Mascolo, G., Bassetti, A., 1999. Thermal treatment of sediments as a function of temperature and reacting atmosphere. J. Anal. Appl. Pyrolysis 52, 115–135. https://doi.org/10.1016/S0165-2370(99)00054-6.

Retzmann, A., Zimmermann, T., Pröfrock, D., Prohaska, T., Irrgeher, J., 2017. A fully automated simultaneous single-stage separation of Sr, Pb, and Nd using DGA Resin for the isotopic analysis of marine sediments. Anal. Bioanal. Chem. 409, 5463–5480. https://doi.org/10.1007/s00216-017-0468-6.

Roux, P., Lemarchand, D., Redon, P.-O., Turpault, M.-P., 2022. B and δ11B biogeochemical cycle in a beech forest developed on a calcareous soil: pools, fluxes, and forcing parameters. Sci. Total Environ. 806, 150396. https://doi.org/10.1016/j.scitotenv.2021.150396.

Rowe, C., Brand, M., Hutley, L.B., Wurster, C., Zwart, C., Levchenko, V., Bird, M., 2019. Holocene savanna dynamics in the seasonal tropics of northern Australia. Rev. Palaeobot. Palynol. 267, 17–31. https://doi.org/10.1016/j.revpalbo.2019.05.004.

Ruiz, J.M., Baghour, M., Bretones, G., Belakbir, A., Romero, L., 1998. Nitrogen metabolism in tobacco plants (nicotina tabacum L.): role of boron as A possible regulatory factor. Int. J. Plant Sci. 159, 121–126.

Ryan, R., Dosseto, A., Dlapa, P., Thomas, Z., Simkovic, I., Mooney, S., Bradstock, R., 2025. Using Fourier transform infrared spectroscopy to produce high-resolution Centennial records of past high-intensity fires from organic-rich sediment deposits. Int. J. Wildland Fire 34. https://doi.org/10.1071/WF23175.

Ryan, R., Dosseto, A., Lemarchand, D., Dlapa, P., Thomas, Z., Simkovic, I., Bradstock, R., 2023. Boron isotopes and FTIR spectroscopy to identify past high severity fires. Catena 222. https://doi.org/10.1016/j.catena.2022.106887.

Ryan, R., Thomas, Z., Simkovic, I., Dlapa, P., Worthy, M., Wasson, R., Bradstock, R., Mooney, S., Haynes, K., Dosseto, A., 2024. Assessing changes in high-intensity fire events in south-eastern Australia using Fourier Transform Infra-red (FITR) spectroscopy. Int. J. Wildland Fire 33, 1–15. https://doi.org/10.1071/WF24064.

Salmona, J., Dixon, K.M., Banks, S.C., 2018. The effects of fire history on hollow-bearing tree abundance in montane and subalpine eucalypt forests in southeastern Australia. For. Ecol. Manage. 428, 93–103. https://doi.org/10.1016/j.foreco.2018.06.026.

Schmidt, M.W.I., Noack, A.G., 2000. Analysis , distribution , implications , and current challenges. Glob. Biogeochem. Cycles 14, 777–793.

Schroeder, P., 2002. Infrared spectroscopy in clay science. Teach. Clay Sci. 11, 182–206.

Seydack, A.H.W., Bekker, S.J., Marshall, A.H., 2007. Shrubland fire regime scenarios in the Swartberg Mountain Range, South Africa: implications for fire management. Int. J. Wildland Fire 16, 81–95. https://doi.org/10.1071/WF06015.

Shakesby, R.A., Wallbrink, P.J., Doerr, S.H., English, P.M., Chafer, C.J., 2007. Distinctiveness of wildfire effects on soil erosion in south-east Australian eucalypt forests assessed in a global context. For. Ecol. Manage. 238, 347–364. https://doi.org/10.1016/j.foreco.2006.10.029.

Shapchenkova, O.A., Kukavskaya, E.A., Groisman, P.Y., 2024. Fire-Induced changes in geochemical elements of Forest floor in Southern siberia. Fire 7, 243. https://doi.org/10.3390/fire7070243.

Simkovic, I., Dlapa, P., Doerr, S.H., Mataix-Solera, J., Sasinkova, V., 2008. Thermal destruction of soil water repellency and associated changes to soil organic matter as observed by FTIR spectroscopy. Catena 74, 205–211. https://doi.org/10.1016/j.catena.2008.03.003.

Šimkovic, I., Dlapa, P., Feketeová, Z., 2023. Application of Infrared spectroscopy and thermal analysis in explaining the variability of soil water repellency. Appl. Sci. 13. https://doi.org/10.3390/app13010216.

Smidt, E., Eckhardt, K.U., Lechner, P., Schulten, H.R., Leinweber, P., 2005. Characterization of different decomposition stages of biowaste using FT-IR spectroscopy and pyrolysis-field ionization mass spectrometry. Biodegradation 16, 67–79. https://doi.org/10.1007/s10531-004-0430-8.

Thomas, Z.A., Mooney, S., Cadd, H., Baker, A., Turney, C., Schneider, L., Hogg, A., Haberle, S., Green, K., Weyrich, L.S., Pérez, V., Moore, N.E., Zawadzki, A., Kelloway, S.J., Khan, S.J., 2022. Late Holocene climate anomaly concurrent with fire activity and ecosystem shifts in the eastern Australian highlands. Sci. Total Environ. 802, 149542. https://doi.org/10.1016/j.scitotenv.2021.149542.

Turney, C., Becerra-Valdivia, L., Sookdeo, A., Thomas, Z.A., Palmer, J., Haines, H.A., Cadd, H., Wacker, L., Baker, A., Andersen, M.S., Jacobsen, G., Meredith, K., Chinu, K., Bollhalder, S., Marjo, C., 2021. Radiocarbon protocols and first intercomparison results from the chronos 14Carbon-Cycle facility, University of New South Wales, Sydney, Australia. Radiocarbon 63, 1003–1023. https://doi.org/10.1017/RDC.2021.23.

Vogl, J., Rosner, M., 2012. Production and certification of a unique set of isotope and Delta reference materials for boron isotope determination in geochemical, environmental and industrial materials. Geostand. Geoanal. Res. 36, 161–175. https://doi.org/10.1111/j.1751-908X.2011.00136.x.

White, I., Wade, A., Worthy, M., Mueller, N., Daniell, T., White, I., Wade, A., Worthy, M., Mueller, N., Daniell, T., White, I., Wade, A., Worthy, M., Daniell, T., Wasson, R., 2006. The Vulnerability of Water Supply Catchments to bushfires: impacts of the January 2003 wildfires on the Australian Capital Territory. Australas. J. Water Resour 10, 179–194. https://doi.org/10.1080/13241583.2006.11465291.

Worboys, G., 2003. A brief report on the 2003 Australian alps bushfires. Mt. Res. Dev. 23, 294–295. https://doi.org/10.1659/0276-4741(2003)023[0294:abrota]2.0.co;2.

Worthy, M., 2013. A History of Fire and Sediment Transport in the Cotter River Catchment, Southeastern Australia. Australian National University [PhD thesis].

Worthy, M., 2005. High-resolution total stream power estimates for the Cotter river. Namadgi National Park, Australian Capital Territory, pp. 338–343. Regolith.

Wu, J., Porinchu, D.F., 2020. A high-resolution sedimentary charcoal- and geochemistry-based reconstruction of late Holocene fire regimes in the páramo of Chirripó National Park, Costa Rica. Quat. Res. 93, 314–329. https://doi.org/10.1017/qua.2019.64.

Younes, N., Yebra, M., Boer, M.M., Griebel, A., Nolan, R.H., 2024. A review of leaf-level flammability traits in eucalypt trees. Fire 7, 183. https://doi.org/10.3390/fire706018.

Yusiharni, E., Gilkes, R., 2012. Rehydration of heated gibbsite, kaolinite and goethite: an assessment of properties and environmental significance. Appl. Clay Sci. 64, 61–74. https://doi.org/10.1016/j.clay.2011.12.005.

Zaccone, C., Rein, G., D'Orazio, V., Hadden, R.M., Belcher, C.M., Miano, T.M., 2014. Smouldering fire signatures in peat and their implications for palaeoenvironmental reconstructions. Geochem. Cosmochim. Acta 137, 134–146. https://doi.org/10.1016/j.gca.2014.04.018.

Zylstra, P., 2006. Fire History of the Australian Alps: prehistory to 2003. In: Australian Alps Liaison Committee: Canberra, pp. 1–39. https://doi.org/10.4135/9781446247501.n1476.